Diamond & Related Materials 117 (2021) 108474

Contents lists available at ScienceDirect

Diamond & Related Materials

journal homepage: www.elsevier.com/locate/diamond

Diamond-doped silica aerogel for solar geoengineering

Jovana Vukajlovic [a,*], Jiabin Wang [a], Ian Forbes [b], Lidija Šiller [a]

[a] School of Engineering, Newcastle University, Newcastle upon Tyne NE1 7RU, UK
[b] Department of Physics and Electrical Engineering, Northumbria University, Newcastle upon Tyne NE1 8ST, UK

ARTICLE INFO

Keywords:
Diamond
Doping
Silica aerogel
Engineered aerosols

ABSTRACT

Even though aerosol injection into stratosphere is one of the most promising solar geoengineering techniques, sulfate aerosols, which are suggested for such an application, show significant drawbacks such as infra-red (IR) absorption and ozone degradation. The development of new materials for such application that would exhibit substantial up-scattering, with non-IR absorption to allow a cooling effect are needed. Here, a novel composite material comprised of diamonds dispersed in a silica aerogel network is investigated and compared to pure silica aerogel. Silica aerogels are ultralight, highly porous, transparent and can host particles, while fulfilling particle size limitation in terms of potential health risks for humans during respiration. Morphology of both the diamonds and the silica aerogels composites has been studied. The diffuse reflectance of the diamond powders, pure silica aerogels, and the diamond-doped silica aerogels have been measured for comparison. Our experimental work assesses the proposed concept of materials, including discussion and recommendations for the improvements of the synthetized materials. The obtained results are promising and could stimulate further in-depth studies in similar materials with a potential for applications in solar geoengineering.

1. Introduction

Geoengineering has emerged as a tool to mitigate global warming by either direct carbon dioxide removal or solar radiation management (SRM) [1]. Mount Pinatubo (Philippines) erupted in 1991 releasing sulphur dioxide in the atmosphere. From there, sulfate aerosols as H_2O-H_2SO_4 droplets were formed, which scattered solar radiation from the Earth. Following the volcanic eruption, a short-lived reduction in global temperature of ~0.5 K was observed in 1992, only for the temperature to return to the value prior to the eruption in 1995 [2]. Although the cooling effect was recorded shortly after the volcanic event, long-term risks of such sulfate aerosols remain. As a consequence of a high aerosol concentration, large particles form by condensation, decreasing the effectiveness of the aerosol [3] and shortening the aerosol life-time due to faster settling [4]. In addition, such aerosols can cause acid rain, catalyse the degradation of ozone, and result in a decrease in solar panel productivity [3]. Nevertheless, the cooling effect of sulfate aerosols has inspired the aerosol injection technique to become one of the most prosperous SRM methods due to its cost-effectiveness and potential rapid deployment [5].

Titania (anatase and rutile phase), silicon carbide, diamond, alumina, silica, zirconia, calcite, soot, and sulfuric acid were previously proposed to be used as geoengineering aerosols and were included in various theoretical models [6–8]. Keutsch's group from Harvard University has launched Stratospheric Controlled Perturbation Experiment (SCoPEx) using calcite ($CaCo_3$) to study the effect of these aerosols on the atmosphere [9,10]. High refractive index aerosols are believed to significantly improve up-scattering, and in case of diamond particles between 0.05 and 0.7 μm are predicted to be the most efficient [6].

Although both silica and diamond have been proposed for geoengineering aerosols with intention to reflect light and subsequently reduce heating, they have never been combined or compared. The novel composite could benefit from the good properties of individual materials. Diamond has exceptional properties such as a high refractive index ($n = 2.41$ [6]), does not absorb IR, and it is non-toxic (biocompatible) [11]. It is thus believed that it might outperform other proposed aerosol materials. Silica aerogel is ultra-porous, light, transparent, low cost and non-toxic [12]. Silica aerogels have recently been proposed to be used in space engineering because they strongly attenuate harmful UVA and UVB radiation (280–400 nm) [13] and another study showed that it does not degrade under UV exposure [14]. Additionally, silica was determined to be suitable for doping with various nanoparticles, where the

* Corresponding authors at: EPSRC Centre for Doctoral Training in Diamond Science and Technology, University of Warwick, Gibbet Hill Road, Coventry CV4 7AL, UK.
E-mail addresses: j.vukajlovic2@newcastle.ac.uk (J. Vukajlovic), Lidija.siller@ncl.ac.uk (L. Šiller).

https://doi.org/10.1016/j.diamond.2021.108474
Received 18 February 2021; Accepted 1 May 2021
Available online 27 May 2021

nanoparticle optical properties are sustained in the final material [15]. The composite structures made of silica aerogels with different carbon nanostructures in the form of nanotubes, nanofibers, and graphene have also been developed [16]. In addition, $PM_{2.5}$ aerosols (particles smaller than 2.5 μm) are considered harmful for humans during respiration. Nevertheless, it is suggested that the aerosol particles should be within a size range of ~0.1–1 μm in order to minimise health risks [17].

The silica aerogel powders can be now produced on a large scale by low cost at ambient pressure drying processing, due to usage of low cost solvents [18–20]. In addition, diamond powders (prepared by high pressure high temperature (HPHT) and detonation synthesis) can be purchased in ton quantities, at low cost. In addition, diamond-silica composite materials, with ultra-light weight are expected to stay longer in the atmosphere than pure diamonds before settling (see further discussion in the paper), and by using diamond particles smaller than 100 nm as dopants this material could also ensure that the overall particle range is within 0.1–1 μm range.

A well-known fact is that the blackbody radiation emission from Sun and Earth peaks in the UV/Vis and IR range of the electromagnetic spectrum, respectively [21]. The solar aerosols therefore enable cooling by scattering of the Sunlight in the shortwave and transmission of the Earth's radiation in the longwave spectrum range. The idea guiding this concept is that silica aerogel would serve as a host and act as lower-cost scatterer, while diamond dopant would be a highly efficient up-scatterer with improving the IR transmittance.

The aim of this work is to measure the reflectance of diamond in silica aerogels, encouraged by the aforementioned theoretical models suggesting potential use of these materials in solar geoengineering [6]. The current work focuses on bulk measurements of the prepared aerogel in a form of a granulated layer. By grinding and size selection of the diamond-doped silica aerogel solid atmospheric aerosols could be obtained, which could be used for solar scattering [5]. The obtained results from this work can be used as a starting point to evaluate the proposed novel composite material and offer insight for the possible further future improvements.

2. Experimental methods

2.1. Materials

Raw diamond powder (in size range 0–2 μm, prepared by high pressure high temperature (HPHT) diamonds supplied by Element6), ethanol (absolute, Fisher), tetraethyl orthosilicate (TEOS, 98%, Sigma Aldrich), ammonium hydroxide-NH_4OH (28–30%, Sigma-Aldrich), ammonium fluoride-NH_4F (98%, Sigma-Aldrich), and hexane (95%, Sigma Aldrich) were used for the experiments. Deionised water (DI water) was obtained from Barnstead™ Nanopure™ (Thermo Scientific) for purification with 18.2 MΩ·cm resistivity.

2.2. Aerogel synthesis

The silica aerogel samples in this paper were prepared according to the adapted procedure from the literature [22] that was used for doping silica aerogels with nickel nanoparticles (NiNPs). Here, silica aerogel was doped with raw diamonds (0–2 μm) instead of NiNPs. In short, as-received diamond powder was added to the mixture solution before gelation at a concentration of 900 ppm (by weight). TEOS was used as a precursor, along with ethanol, and deionised water at a molar ratio of 2:38:39, respectively. Firstly, raw diamonds were ultra-sonicated for 4 min in DI water, after which, the diamond solution was added to the TEOS, ethanol, and catalyst (molar ratio is NH_4OH:NH_4F:H_2O = 8:1:111). In terms of the pure aerogel, DI water, TEOS, ethanol, and catalyst, without the addition of diamond, were mixed. After the precursor solution and diamond mixture (30 ml) was sufficiently mixed it was subsequently transferred to a mould and left for about 10 min to facilitate gelation. After the hydrogel was obtained, the mould was removed and ethanol was added for aging. After 24 h, ethanol was exchanged for hexane (500 ml) in the solvent exchange step, by pouring out ethanol and adding hexane, followed by another two hexane exchanges. After the third hexane exchange, the gel was left on a hot plate at 60 °C to dry, after which the aerogel was collected. The pure silica aerogel was transparent, while the doped aerogel appeared milky white. The pristine silica aerogel was labelled as 'pure silica aerogel' and the silica aerogel doped which contained 900 pm of the raw diamond powder was referred to as '900 R'. 900 ppm of diamond particles in aerogels was chosen for the optical measurements because this was our highest achievable concentration of diamonds in aerogels, without sedimentation during gelation process.

2.3. Characterisation

The size of the diamond particles was characterized by dynamic light scattering (DLS) using Zetasizer Nano ZS (Malvern Instruments). The powders were dispersed in DI water and the DLS measurement was conducted at 25 °C with a 173° scattering angle. LabRAM HR800 with a 514.5 nm Ar green laser was used to measure the Raman spectra (100–2000 cm^{-1}) of the diamond powder. Diamond particles were deposited on silicon wafers from the ethanol suspensions.

FTIR spectroscopy of the diamond powder and the silica aerogel fine powders was obtained by using an IRAffinity-1s Spectrophotometer (Shimadzu), where a spectrum energy range of 500–4000 cm^{-1} was scanned. Scanning electron microscopy (SEM, JEOL5300) of the pure diamond powder was conducted with an accelerating voltage of 10 kV. A BIO-RAD Microscience division SC500 sputter coater was used in order to coat the aerogels with Au and then SEM analysis was conducted by a Philips XL series ESEM using a 10 kV accelerating voltage (with high magnifications from 25,000 to 100,000). Lacey carbon films on a 300 copper mesh grids were used to obtain transmission electron microscopy (TEM, Hitachi HT7800) images of both the diamond powders and silica samples, with a 100 kV accelerating voltage. X-ray diffraction (XRD) patterns of the pure diamond powders and powdered aerogels composite were obtained by a PAN-alytical X'Pert Pro diffractometer (with Cu $\lambda = 1.540$ Å). The spectra were fitted using HighScore Plus software. The quantitative analysis was preformed using Rietveld refinement. A ThermoScientific Surfer system was used to determine the specific surface area, pore size distribution and pore volume of the samples. The specific surface area was found by measuring the adsorption of gaseous N_2 using Brunauer-Emmett-Teller (BET) analysis. Pore distributions were obtained from the nitrogen adsorption/desorption isotherms by the Barrett-Joyner-Halenda (BJH) method. Bulk densities were measured as a ratio of the weight to volume followed by porosity calculations for both silica aerogels. All characterisation techniques listed above, as well as the synthesis procedures, were carried out at Newcastle University. The diffuse reflectance was done by spectrophotometer (Shimadzu SolidSpec-3700 UV–Vis-NIR, 290–2600 nm) using UVProbe software at Northumbria University. The instrument incorporates three detectors as follows: a photomultiplier tube (PMT), InGas, and PbS detectors for the UV, Vis, and near-infrared regions, respectively. A slow scan speed and a 20 nm slit width were used during detection. A thin film of fine aerogel powders, as well as the pure diamond powder and powdered composites, were deposited in the cavity of the glass slide and then covered with a glass cover slip prior to the optical measurements being conducted.

3. Results and discussion

SEM, TEM, and DLS measurements of the diamond powder were conducted in order to observe the particle size and size distribution of the raw diamond powder (Fig. 1a-d). DLS was used to determine the average particle size (Fig. 1b). The number distribution has a peak at 295 nm, while the *Z*-average is 552.1 ± 7.35 nm. This suggests that although the particles cover a broad size range from about 150–2000

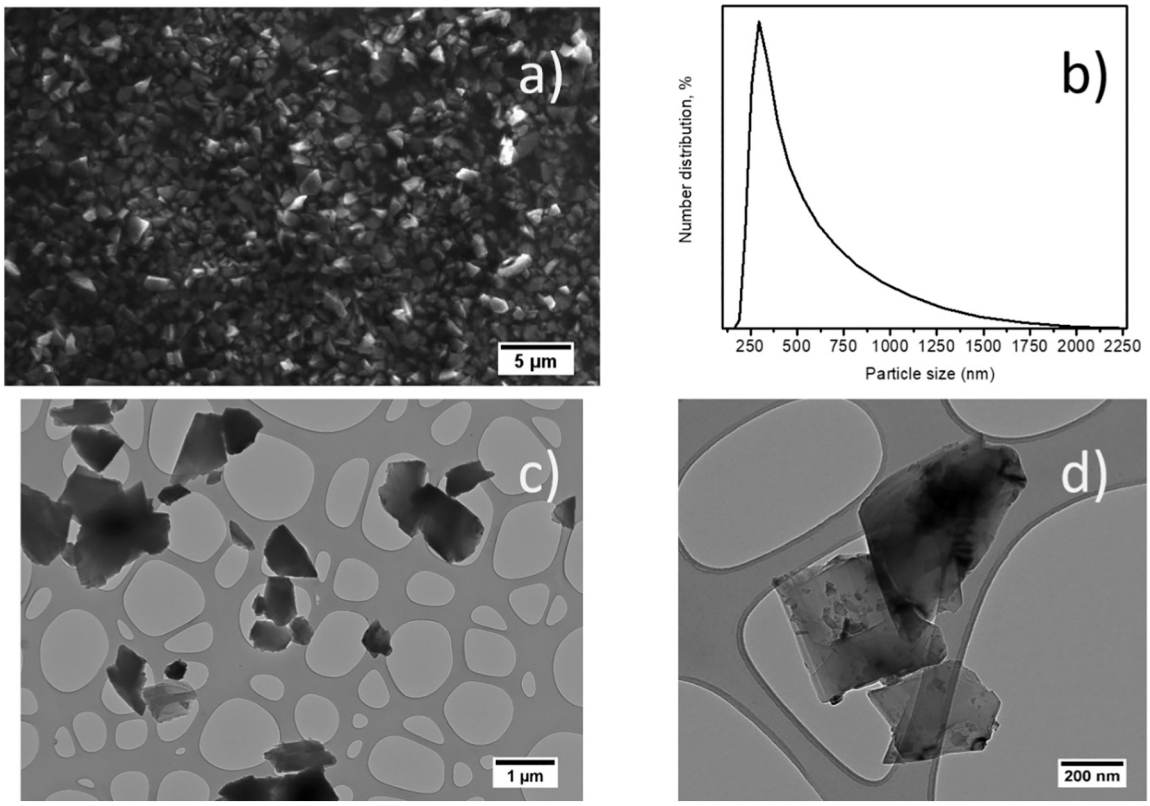

Fig. 1. a) SEM image of the raw diamond powder, b) DLS particle size distribution of the raw diamond powder, and c) and d) TEM images of the raw diamond powder.

nm, the great majority of the particles are below 1 µm. SEM (Fig. 1a) and TEM images (Fig. 1c/d) of the diamond powder show particles of irregular size with sharp edges. The SEM image, as well as TEM images, are in good agreement with DLS measurements that show a broad size distribution of particles of the diamond powder. These results also confirm that the raw diamond particles are within a size range of 0–2 µm, as stated by the supplier.

The surface of the diamond particles, as well as the diamond purity, were assessed by Raman scattering spectroscopy (Fig. 2). The feature related to the cubic phase of diamond appears at 1332 cm^{-1} [23,24]. The absence of graphitic peaks at 1350 cm^{-1} (D-band) and 1590 cm^{-1} (G-band) [23] in the Raman spectrum suggests that the diamond powder has no graphitic carbon (sp^2) on the surface of the diamond particles and shows that the raw diamond powder has a high level of purity. FTIR also examined the surface of diamond powder, where only air contaminants such as water and CO_2 were observed (see section S1, supplementary materials).

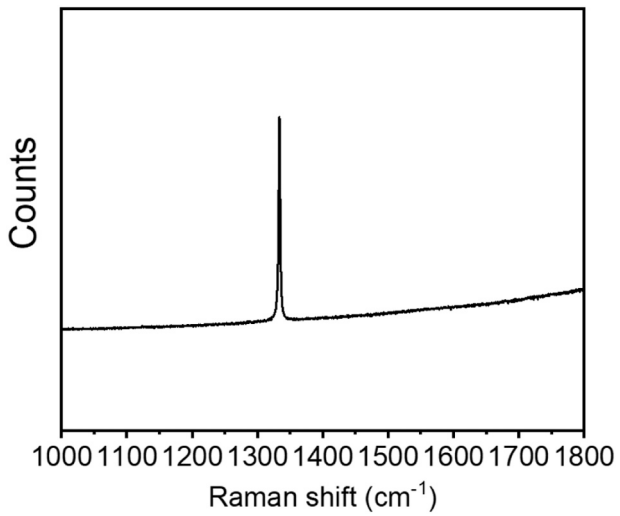

Fig. 2. Raman scattering spectrum of the raw diamond powder.

The microstructure and surface of the silica aerogels, pure and diamond-doped, were examined by SEM. Diamond particles could not be observed by SEM, due to the fact that they were covered by silica aerogels. As such, the pure and diamond-doped silica aerogels both resembled one another. The SEM images of pure silica aerogel is presented in Fig. 3a, where a typical porous aerogel structure is observed. The TEM image of the pure silica aerogel (Fig. 3b) is in agreement with the SEM image of the pure silica in terms of a high porosity and a grape-like structure. The darker areas in Fig. 3b are due to the overlapping layers of silica particles which form the networking microstructure of the aerogel. The diamond-doping of silica aerogel was captured by TEM (Fig. 3c) which shows that the silica aerogel contains a diamond particle with a length of ~500 nm. Diamond particles maintain their sharp edges, size, and irregular shape which is consistent with the diamond images prior to doping, as seen in Fig. 1c and d. The influence of the incorporation of diamond on the nanoporosity of silica will be discussed later in this paper.

Fig. 4a and b represents the XRD patterns of pure and diamond-doped silica aerogel. All silica aerogels have a broad, amorphous peak at ~22° [25], while the doped aerogel shows three additional crystalline diamond peaks. An XRD pattern of the pure diamond powder can be seen in Fig. 4 (as insert). The diamond peaks correspond to the cubic diamond structure with the following diamond planes [26]: 44° (111), 75.4° (220), and 91.4° (311). The diamond powder contains small amounts of contaminants such as aluminium manganese titanium alloy and cobalt zinc carbide. On the other hand, no graphitic peak (002) at $2\theta = 27°$ [27] was observed, which is in agreement with the Raman measurements that the diamond is of a good quality and purity.

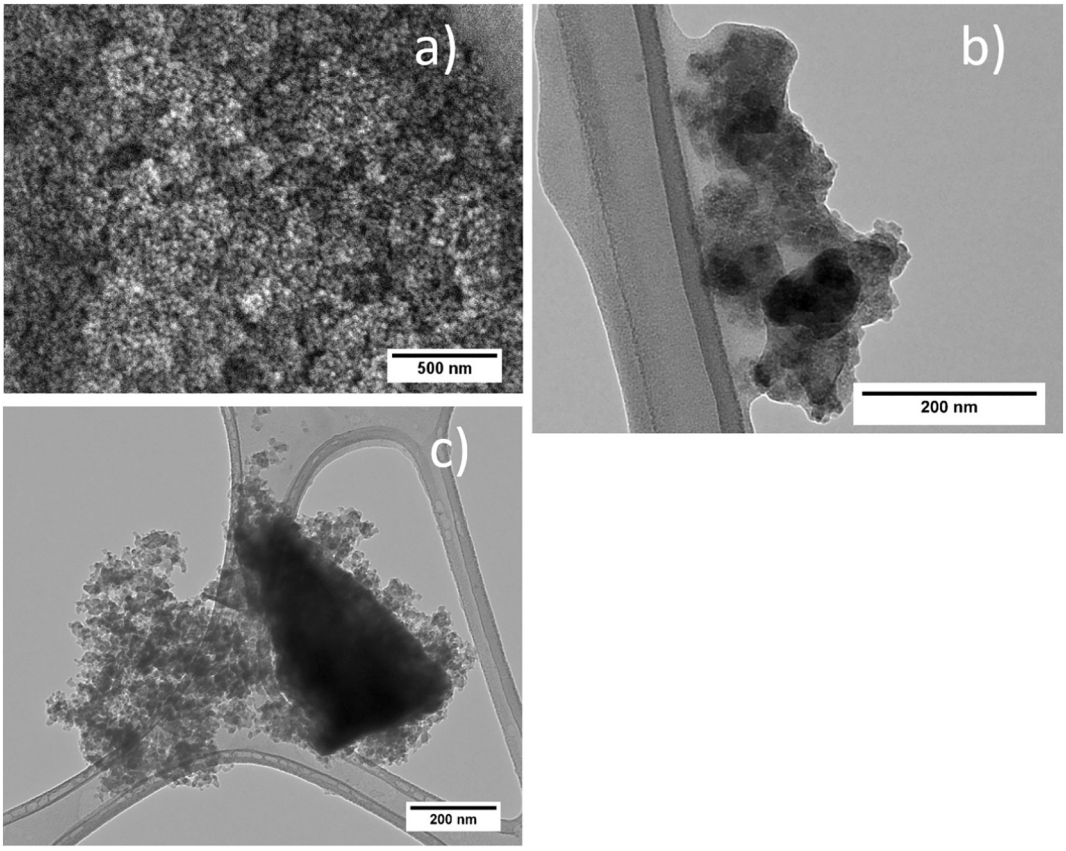

Fig. 3. a) SEM images of the pure silica aerogel, and TEM images of: b) pure silica aerogel, and c) raw diamond-doped silica aerogel.

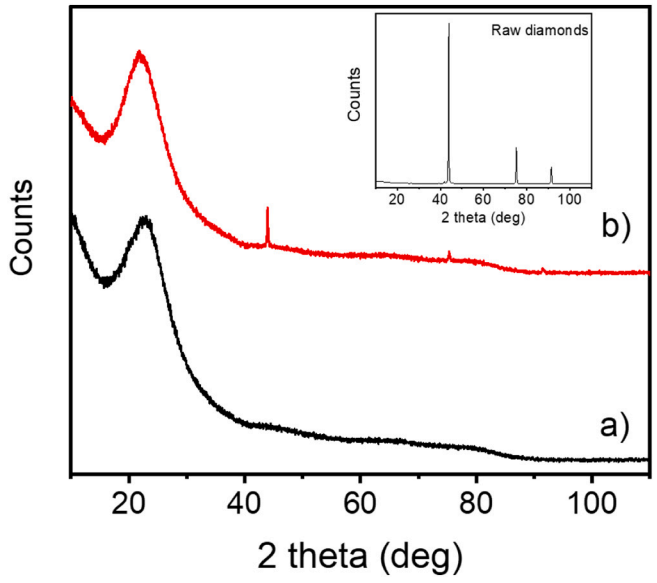

Fig. 4. XRD pattern of: a) pure silica aerogel and b) raw diamond-doped silica aerogel and raw diamond powder (as insert).

Furthermore, the XRD pattern of the diamond-doped aerogel confirms the observed diamond-doping of silica aerogel, evidenced by TEM. Additionally, a quantitative analysis was used to determine the final concentration of diamond in the silica aerogels after drying, which was determined to be 3.3 wt%. The remaining 96.7 wt% in the doped aerogels corresponds to amorphous silica.

The mass per volume was determined and along with the skeletal density, porosity of the aerogel samples was calculated. The skeletal density was determined to be 2.65 g/cm^3 for the pure aerogel, whereas the doped aerogel exhibited a higher skeletal density of 2.68 g/cm^3, due to diamond-doping. The mass per volume for the pure aerogel (0.281 g/cm^3) is lower than that of the doped aerogel (0.368 g/cm^3). The amount of catalyst used for the doped aerogels is higher due to the necessity of speeding up the gelation process in order to mitigate diamond particle accumulation and sedimentation, which inevitably leads to a higher bulk density of the resulting doped sample. Consequently, the porosity of the doped aerogel (86.3%) was calculated to be lower than that of the pure silica aerogel (89.4%).

The BET surface area and BJH pore size calculations provided the surface area, the specific pore volume, and the average pore diameter for the pure and doped silica aerogels (see section S2, supplementary material). The pure silica aerogel was determined to have a surface area of 544 m^2/g, with a specific pore volume of 1.84 cm^3/g, and an average pore diameter of 12.0 nm. For the doped silica aerogel, the surface area was determined to be 284 m^2/g, along with a specific pore volume of 2.22 cm^3/g, and average pore diameter of 20.2 nm. The increased amount of catalyst and incorporation of diamond is believed to result in a decrease in the surface area, as well as an increase in the pore volume and the pore diameter of the silica aerogel composite. The addition of either base catalyst such as NH_4OH or Lewis base catalyst such as NH_4F, will favour the formation of the colloidal aerogel [28]. Here, however, the effect of the increased catalyst amount on the aerogel structure has not been observed in case of the pure and the doped aerogel.

In order to compare the chemical bonding and surface termination of pure and doped aerogels, FTIR spectroscopy was used (see S3 section, supplementary material). Both aerogels show distinctive silica aerogel bands. Furthermore, the spectra are similar to the typical FTIR spectrum of hydrophilic silica aerogel [29]. Water (~1500 cm^{-1} and ~3500 cm^{-1}) and carbon dioxide (~2300 cm^{-1}), originating from the ambient

air, also appear in the spectrum. Bands at 800 cm^{-1} and 1075 cm^{-1} are related to the O-Si-O symmetric and asymmetric vibrations [30], respectively. The presence of Si-OH groups on the surface is confirmed by the 550 cm^{-1} and 960 cm^{-1} bands [30].

Fall speed for the diamond, pure aerogel and diamond-doped silica aerogel particles has been estimated in Supplementary material, see section S4. In summary, average fall speed for pure diamond, silica aerogel and doped silica aerogels estimated from their measured density from this work and their equivalent size, were 0.0219, 0.0070 and 0.0092 cm/s, respectively. Average time that they will stay in atmosphere for pure diamond, silica aerogel and doped silica aerogels was estimated to be 1057, 3306 and 2516 days, respectively. It is clear, that aerogel and aerogel composite materials, both have high porosity and low density, which is suitable for the geoengineering application, because it significantly prologues their stay in the atmosphere.

The silica aerogel prepared as a fine powder is presented in Fig. 5, where particles cover the wide range of sizes from some being smaller than 1 μm to those bigger than 20 μm. Films made of fine powder aerogels particles were also optically measured.

Fig. 6 shows the total diffuse reflectance plot for a) the glass slide, b) raw diamond powder, c) pure silica aerogel, and d) diamond-doped silica aerogel. The glass slide, without a sample, was also scanned to account for the sample holder reflectance. Photos of films of fine powders, prepared for reflectance measurements, are presented in supplementary material, see section S5. Raw powder, pure silica aerogel, and diamond-doped silica aerogel samples all exhibited a reflectance between 30 and 50%, out of which the glass slide contribution to the reflectance is only a couple of percent. We can see that pure diamonds decrease reflectance in the UV/Vis (280–600 nm), while improving the reflectance in the NIR (>2000 nm), when compared to pure silica aerogel. This is a bit surprising outcome, but can be explained because the diamond powder appears brown in colour, so increased absorption in the Vis region is expected, and therefore the subsequent reduction of the reflectance. Diamonds (without impurities and defects) generally will not absorb in the wavelength range of 225 nm to 1 mm and its structural symmetry leads to non-IR absorption [31]. However, this absorption edge can be shifted to a wavelength of 290 nm, when nitrogen impurities are present [32]. These nitrogen defects might have been introduced into the diamond powder during a high pressure high temperature (HPHT) synthesis. The nanoporous structure of silica aerogels gives rise to Rayleigh scattering, which is more intense for shorter wavelength scattering when the sunlight is passing through [33]. Hence, the high reflectance of silica aerogel in the region of ~280–400 nm was measured. From there, the silica aerogel reflectance decreases from ~400–800 nm because the transmission in this range increases towards longer wavelengths [34]. Also, it suggested that Mie scattering of the incoming radiation contributes to the reflectance in case of diamond

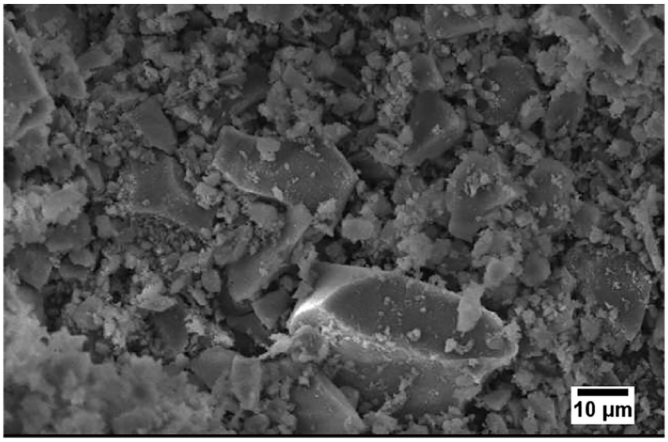

Fig. 5. SEM images of fine powder silica aerogel.

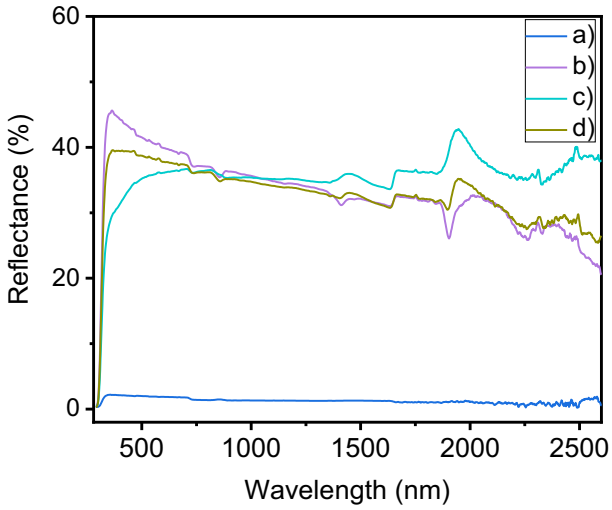

Fig. 6. Reflectance spectra of: a) glass slide only, b) pure aerogel, c) raw diamond, and d) raw diamond-doped silica aerogel.

particles and the white fine powder silica aerogel, which is not strongly wavelength dependent. The bands associated with the regions ~1400 nm and ~1900 nm are related to water and CO_2 absorption and appear only in silica aerogel reflectance patterns [35,36]. The gratings change at 720 nm, while detectors switch at ~870 nm and 1650 nm and these show as features in the spectra [37]. The combination of O—H and Si—O in the structure gives rise to the ~2300 nm and 2500 nm bands [35,38,39]. These two absorptions are typical for silica aerogel. It can be seen that with the addition of diamond these two bands have a lower intensity. Taking into account that only ~3 wt% of diamond is added to the silica aerogel, the impact of diamond on the final reflectance of the doped-silica aerogel in the ~2300–2500 nm reflectance range is significant. Therefore, diamond justifies the theoretical predictions [6] about improving non-absorption in the NIR region. However, silica aerogel alone showed the highest reflectance in the UVA/UVB (280–400 nm) range. This suggests that silica aerogel would reflect this harmful radiation back into space and lessen the amount of UVA/UVB radiation that reaches the Earth's surface. The combination of silica aerogel doped with diamond improves the up-scattering NIR light, in comparison to silica aerogel samples alone.

4. Conclusion

In this work, a diamond-doped silica aerogel for solar geoengineering has been successfully synthesized for the first time to the best of our knowledge. After doping with diamonds (particle size ~500 nm), silica aerogel remained porous, with a low density, and a high surface area. For the intended application of the doped aerogel as a solar aerosol material, a 1 μm composite size, observed by TEM, fulfils the prerequisite safety condition concerning particle inhalation. Reflectance of the prepared composite was measured to investigate the effect of the diamond doping on the optical properties of the silica aerogel.

Due to its nanostructured composition, silica aerogel alone contributes to the highest scattering which is evident in the UVA/UVB/Vis wavelength range, whereas the diamond particles and diamond-doped silica aerogels allow improved scattering in the NIR radiation range. As for the UV/Vis region, composite shows lower reflectance compared to pure silica aerogel. Possible reason is that the HPHT diamonds often contain non-fluorescent isolated nitrogen atoms in the diamond lattice that absorbs above about 550 nm [40]. So we suggest that one possibility in the future would be to use higher quality diamond particles, which could improve further the up-scattering in the UV/Vis. Ultimately, the reflectance data support the use of silica aerogel alone as a good

scatterer in the UV/Vis, while the optimization of the diamond-doping is promising to further enhance the scattering in the UV/Vis and the transmission in the IR.

Importantly, the proposed composite design offers an opportunity to conduct a comparative optical study with smaller sized diamonds (nanoparticles, <100 nm), where silica aerogel would serve as a matrix in order to maintain the aerosol particle size in the safer range (0.1–1 μm). Additionally, narrower size selection of the diamond dopant, as well as the doped aerogel, would allow measurement that can account for the specific particle size-reflectance relationship. In addition, due to the much lower density of aerogels compared to the density of diamonds, silica aerogels and silica aerogel diamond composite materials can provide substantially longer lifetime of aerosols in the stratosphere before they sediment and fall. This work we believe can give incentive to further research into the aerosol geoengineering field, in particular stratospheric chemistry and safety of the proposed diamond-doped silica aerosols based on the surface group interaction with resident stratospheric particles.

Declaration of competing interest

The authors declare that they have no known competing financial interests or personal relationships that could have appeared to influence the work reported in this paper.

Acknowledgments

This work was funded by UK Engineering and Physical Sciences Research Council (EPSRC) Centre for Doctoral Training in Diamond Science and Technology- grant number EP/L015315/1. We thank Mr. Stephen Laidler for critical reading of the manuscript. JV thanks Dr. X. Han for showing her the preparation method of aerogels that is following the ref. [22].

Appendix A. Supplementary data

Supplementary data to this article can be found online at https://doi.org/10.1016/j.diamond.2021.108474.

References

[1] (London), T.R.S, Geoengineering the Climate Science, Governance and Uncertainty, The Royal Society, London, 2009.
[2] M.S.D.P. Gomes, M.S.M. de Araújo, Artificial cooling of the atmosphere—a discussion on the environmental effects, Renewable and Sustainable Energy Reviews 15 (1) (2011) 780–786.
[3] A. Robock, Stratospheric aerosol geoengineering, in: AIP Conference Proceedings, American Institute of Physics Inc, 2015.
[4] P.J. Crutzen, Albedo enhancement by stratospheric sulfur injections: a contribution to resolve a policy dilemma? Climatic Change 77 (3-4) (2006) 211–220.
[5] V.F. McNeill, Atmospheric aerosols: clouds, chemistry, and climate, Annu Rev Chem Biomol Eng 8 (2017) 427–444.
[6] D.K. Weisenstein, D.W. Keith, J.A. Dykema, Solar geoengineering using solid aerosol in the stratosphere, Atmospheric Chemistry and Physics 15 (20) (2015) 11835–11859.
[7] F.D. Pope, et al., Stratospheric aerosol particles and solar-radiation management, Nature Climate Change 2 (10) (2012) 713–719.
[8] J.A. Dykema, D.W. Keith, F.N. Keutsch, Improved aerosol radiative properties as a foundation for solar geoengineering risk assessment, Geophysical Research Letters 43 (14) (2016) 7758–7766.
[9] D.W. Keith, et al., Stratospheric solar geoengineering without ozone loss, Proc Natl Acad Sci U S A 113 (52) (2016) 14910–14914.
[10] Group, K, SCoPEx: Stratospheric Controlled Perturbation Experiment [cited 2021 11.02.2021]; Available from: https://www.keutschgroup.com/scopex, 2021.
[11] V.N. Mochalin, et al., The properties and applications of nanodiamonds, Nat Nanotechnol 7 (1) (2011) 11–23.
[12] H. Maleki, L. Durães, A. Portugal, An overview on silica aerogels synthesis and different mechanical reinforcing strategies, Journal of Non-Crystalline Solids 385 (2014) 55–74.
[13] R. Wordsworth, L. Kerber, C. Cockell, Enabling Martian habitability with silica aerogel via the solid-state greenhouse effect, Nature Astronomy 3 (10) (2019) 898–903.
[14] E. Strobach, et al., High temperature stability of transparent silica aerogels for solar thermal applications, APL Materials (2019) **7**(8).
[15] C. Ziegler, et al., Modern inorganic aerogels, Angew Chem Int Ed Engl 56 (43) (2017) 13200–13221.
[16] A. Lamy-Mendes, R.F. Silva, L. Durães, Advances in carbon nanostructure–silica aerogel composites: a review, Journal of Materials Chemistry A 6 (4) (2018) 1340–1369.
[17] J.M. Benson, Safety consideration when handling metal powders, The Journal of The Southern African Institute of Mining and Metallurgy 112 (7) (2012) 563–575.
[18] X. Han, et al., Bioinspired synthesis of monolithic and layered aerogels, Adv Mater 30 (23) (2018), e1706294.
[19] S. De Pooter, et al., Optimized synthesis of ambient pressure dried thermal insulating silica aerogel powder from non-ion exchanged water glass, Journal of Non-Crystalline Solids 499 (2018) 217–226.
[20] S. Zhao, et al., Phase transfer agents facilitate the production of superinsulating silica aerogel powders by simultaneous hydrophobization and solvent- and ion-exchange, Chemical Engineering Journal 381 (2020).
[21] M.Z. Jacobson, Fundamentals of Atmospheric Modeling, 2 ed., Cambridge University Press, Cambridge, 2005.
[22] X. Han, et al., Synthesis and characterisation of ambient pressure dried composites of silica aerogel matrix and embedded nickel nanoparticles, The Journal of Supercritical Fluids 106 (2015) 140–144.
[23] P.H. Chung, E. Perevedentseva, C.L. Cheng, The particle size-dependent photoluminescence of nanodiamonds, Surface Science 601 (18) (2007) 3866–3870.
[24] S. Prawer, R.J. Nemanich, Raman spectroscopy of diamond and doped diamond, Philosophical Transactions of the Royal Society A: Mathematical, Physical and Engineering Sciences 362 (1824) (2004) 2537–2565.
[25] M.V. Khedkar, et al., Surface modified sodium silicate based superhydrophobic silica aerogels prepared via ambient pressure drying process, Journal of Non-Crystalline Solids 511 (2019) 140–146.
[26] D.C. Barbosa, et al., Activation energies for the growth of diamond films and the renucleation of diamond grains during film growth, Journal of Vacuum Science & Technology B, Nanotechnology and Microelectronics: Materials, Processing, Measurement, and Phenomena 32 (3) (2014).
[27] P. Ruvinskiy, et al., Nano-silicon containing composite graphitic anodes with improved cycling stability for application in high energy lithium-ion batteries, ECS Journal of Solid State Science and Technology 2 (10) (2013) M3028–M3033.
[28] M. Aegerter, N. Leventis, M. Koebel, Aerogels Handbook, Springer, New York, 2011.
[29] M. Li, H. Jiang, D. Xu, Preparation of sponge-reinforced silica aerogels from tetraethoxysilane and methyltrimethoxysilane for oil/water separation, Materials Research Express (2018) **5**(4).
[30] E. Vinogradova, M. Estrada, A. Moreno, Colloidal aggregation phenomena: spatial structuring of TEOS-derived silica aerogels, J Colloid Interface Sci 298 (1) (2006) 209–212.
[31] J.W. Tropf, E.M. Thomas, Optical properties of diamond, Johns Hopkins APL Technical Digest 14 (1993) 16–23.
[32] K. Snail, et al., Hemispherical transmittance of several free standing diamond films, in: 33rd Annual Technical Symposium Vol. 1146, SPIE, 1989.
[33] M. Zinzi, et al., Optical and visual experimental characterization of a glazing system with monolithic silica aerogel, Solar Energy 183 (2019) 30–39.
[34] C. Buratti, E. Moretti, Glazing systems with silica aerogel for energy savings in buildings, Applied Energy 98 (2012) 396–403.
[35] M. Rubin, C.M. Lampert, Transparent silica aerogels for window insulation, Solar Energy Materials 7 (4) (1983) 393.
[36] U. Berardi, Development of glazing systems with silica aerogel, Energy Procedia 78 (2015) 394–399.
[37] Shimadzu, Shimadzu UV-VIS-NIR Spectrophotometer, cited, 2020, 14.04.2020.
[38] C. Buratti, E. Moretti, Experimental performance evaluation of aerogel glazing systems, Applied Energy 97 (2012) 430–437.
[39] L. Zhao, et al., Modeling silica aerogel optical performance by determining its radiative properties, AIP Advances 6 (2) (2016).
[40] S. Eaton-Magaña, J.E. Shigley, C.M. Breeding, Observations on HPHT-grown synthetic diamonds: a review, Gems & Gemology 53 (2017) 262–284.